Computational Approach to Ultrafast Hydrogen Bonding in Water and Ice

Author(s)
(Dated: February 13, 2026)

I. INTRODUCTION

The paper is organized as follows: first a brief and general introduction on the GLE is given, focusing on the frequency- dependent coupling between the thermostat and the system; then a first case study, namely, liquid methanol, is presented together with a detailed systematic analysis of technical aspects of the thermostat; finally, we report a second application on liquid water in order to highlight the portability of the method and the physical differences between the two systems.

II. COMPUTATIONAL DETAILS

A. Generation of Equilibrium Samples

Before investigating the non-equilibrium response induced by vibrational excitation, we generated equilibrium reference samples for liquid water, ice Ih, and ice IX using consistent preparation protocols.

The liquid water samples were generated from an equilibrium configuration at ambient temperature, which was replicated to obtain a system of one thousand molecules. The system was generated inside a cubic cell, whose side length was chosen to reproduce an initial target mass density of 1g/cm^3.

In contrast to the liquid phase, the generation of crystalline ice configurations requires explicit control over proton ordering and lattice symmetry, as well as compliance with the Ice Rules. Under these constraints, crystalline ice samples were generated using the GenIce framework [1].
In order to account for different proton orderings, we chose to represent two ice phases: the Ih phase, which is the stable proton-disordered form of ice under ambient-pressure conditions, and the IX phase, which corresponds to a proton-ordered crystalline structure. For ice Ih, GenIce was used to generate configurations satisfying the ice rules with disordered proton arrangements consistent with the Ih lattice symmetry. For ice IX, a proton-ordered configuration consistent with the corresponding crystallographic structure was generated, without the need for averaging over multiple proton disorder realizations.

Due to the constraints imposed by the GenIce framework on the construction of periodic crystalline cells, the ice Ih and ice IX unit cells were replicated to obtain supercells containing 3072 and 2880 atoms, respectively. These system sizes were chosen as the closest multiples compatible with the underlying lattice symmetries and comparable to the system size used for liquid water.

B. Interaction Model and Computational Framework

All molecular dynamics simulations in this study were performed using a neural network interatomic potential of the NEP (Neuro-Evolution Potential) class. The NEP framework represents the total energy of the system as a sum of atomic contributions expressed as functions of the local environment, with parameters trained on density functional theory (DFT) reference data. This class of potentials has been shown to provide near first-principles accuracy while retaining the computational efficiency required for large-scale molecular dynamics simulations, and has been validated for both liquid water and crystalline ice phases [2]. The simulations were carried out using the GPUMD package, which provides a native implementation of NEP potentials and enables efficient GPU-accelerated molecular dynamics. All equilibrium and non-equilibrium trajectories discussed in this work were generated within this computational framework.

C. Simulation Protocol

For each system, an equilibration stage was first performed to ensure thermodynamic stability prior to the excitation procedure. Equilibration was carried out in the isothermal–isobaric (NPT) ensemble. The temperature was controlled using a Nosé–Hoover chain thermostat, while pressure was regulated through a Berendsen barostat, allowing the simulation cell to relax to the target density. Liquid water was equilibrated at 300 K, whereas the crystalline ice phases were equilibrated at 200 K. Equilibrium was assessed by monitoring the stability of the total energy, temperature, and pressure over time.

At the end of the equilibration stage, the final configuration was used as the reference structure for the excitation protocol. Quantum nuclear fluctuations were incorporated through a Wigner phase-space representation applied to selected vibrational degrees of freedom. The corresponding distribution was constructed from the

eigenstates of the full Lippincott–Schroeder (LS) potential for hydrogen-bonded pairs [3]. The one-dimensional Schrödinger equation associated with the LS potential was solved to obtain the vibrational eigenfunctions and eigenvalues, which were used to evaluate the phase-space distribution.

A fraction corresponding to 10% of the total water molecules was randomly selected and initialized quantum mechanically. For each selected molecule, initial positions and momenta were sampled from the phase-space distributions associated with the $n = 0$ and $n = 1$ vibrational eigenstates of the LS potential for the two O–H bonds, respectively. The remaining 90% of the molecules were initialized according to the classical Maxwell–Boltzmann distribution at the equilibration temperature.

After the excitation step, the system was propagated in the microcanonical (NVE) ensemble to prevent artificial energy exchange with an external thermostat and to enable an unbiased characterization of the intrinsic non-equilibrium response. The subsequent dynamics were followed over a time interval of 30 ps, sufficient to capture both the prompt structural response and the subsequent energy redistribution processes.

All trajectories were integrated using a time step of 0.1 fs, chosen to accurately resolve the high-frequency O–H stretching vibrations and to ensure stable energy conservation during the microcanonical production runs.

For each phase, the entire equilibration–excitation–production workflow was repeated 50 times independently. All reported structural and dynamical observables were obtained by averaging over these independent realizations, and the associated uncertainties were estimated from the corresponding ensemble fluctuations.

III. RESULTS AND DISCUSSION

In the following, we analyze the non-equilibrium response induced by the vibrational excitation through three complementary observables: the vibrational density of states (VDOS), the time-resolved modal temperatures, and the structural evolution of the hydrogen-bond network as characterized by radial distribution functions (RDFs). We first examine the VDOS to verify the effective population of the targeted vibrational states, before addressing the subsequent energy redistribution and its structural consequences.

To resolve the transient spectral evolution following excitation, the VDOS was evaluated over sliding temporal windows of fixed duration, allowing us to monitor the redistribution of vibrational energy as a function of time. Since we are dealing with non-equilibrium trajectories, particular care was taken in selecting the window length used to compute the velocity autocorrelation function

(VACF). Convergence tests showed that the VACF decays to negligible values within approximately 100 fs for all phases considered. Accordingly, a window length of 100 fs was adopted for the VDOS evaluation, ensuring that the correlation function was fully contained within each time segment.

While the time-resolved VDOS provides direct spectral information on the excited vibrational states, its temporal resolution is intrinsically limited by the finite window length required for a stable Fourier transform. To achieve a more refined characterization of the energy redistribution dynamics, we therefore analyze the time evolution of modal temperatures.

The modal temperatures were computed by decomposing the kinetic energy into physically distinct dynamical contributions, including O–H stretching, H–O–H bending, librational motion, hydrogen-bond related motion, and center-of-mass translational degrees of freedom. For each subset of degrees of freedom, an effective temperature was defined through the classical equipartition relation.

More specifically, for each molecule, the instantaneous kinetic energy was projected onto internal and collective coordinates defined at the molecular level.

The stretching contribution was obtained by projecting the relative O–H velocities onto the corresponding bond directions, and the associated modal temperature was defined as

$$T_{\text{stretch}} = \frac{\mu_{OH} v_{\parallel}^2}{k_B}, \tag{1}$$

where μ_{OH} is the reduced mass of the O–H pair and $v_{\parallel}$ is the component of the relative velocity along the bond axis.

The bending contribution was evaluated in terms of the time derivative of the H–O–H angle θ. Defining the bending coordinate as $\phi = \theta/2$, the associated kinetic energy reads

$$K_{\text{bend}} = \frac{1}{2} I_\theta \left(\frac{\dot{\theta}}{2} \right)^2, \tag{2}$$

with $I_\theta = \sum_i m_{H_i} r_{OH,i}^2$ the effective moment of inertia of the two O–H arms. The corresponding modal temperature follows from equipartition as

$$T_{\text{bend}} = \frac{I_\theta \dot{\theta}^2}{4k_B}. \tag{3}$$

Librational contributions were obtained by treating each molecule as an instantaneous rigid body and projecting the angular momentum onto its principal axes. For each rotational degree of freedom α, the associated temperature was defined as

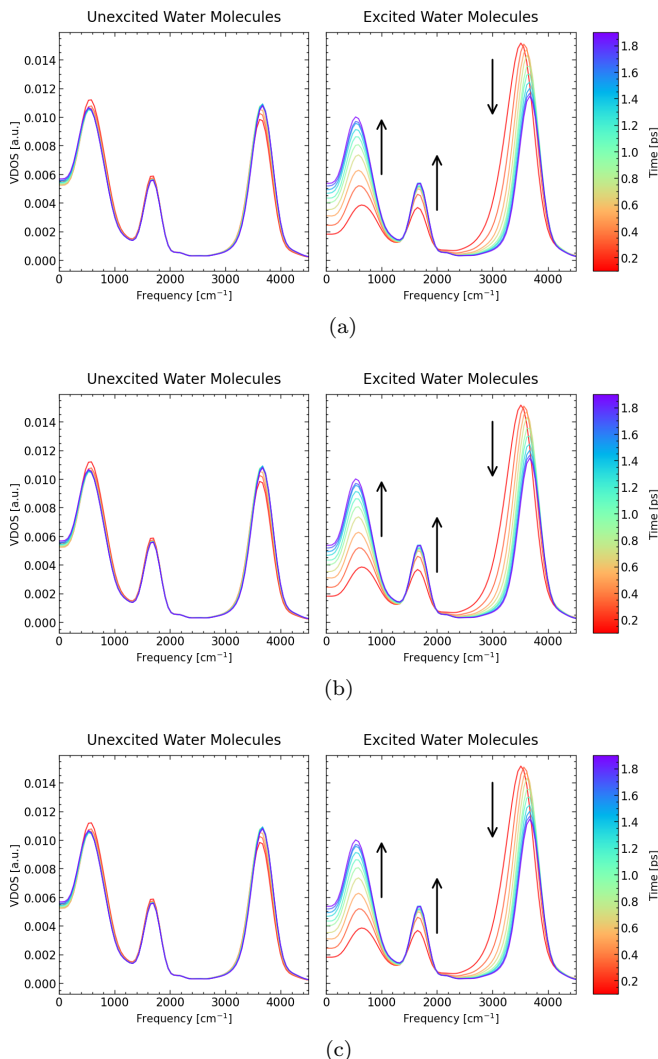$$T_\alpha = \frac{L_\alpha^2}{I_\alpha k_B}, \tag{4}$$

FIG. 1: Time-resolved vibrational density of states
(VDOS) for liquid water under 10% vibrational excita-
tion. The left panel reports the VDOS of non-excited
molecules, while the right panel shows the evolution for
excited molecules. Colors encode the temporal progres-
sion from early (red) to late (blue) times after excita-
tion. The initial enhancement in the O–H stretching
region is centered at the fundamental frequency of the
Lippincott–Schroeder potential and progressively shifts
toward higher frequencies, approaching the equilibrium
stretching band, accompanied by a redistribution of spec-
tral weight toward bending and low-frequency modes.

where L_α and I_α denote the angular momentum compo-
nent and the corresponding principal moment of inertia.

Finally, the center-of-mass and hydrogen-bond contri-
butions were computed from the relative translational
velocities of the corresponding atomic pairs using the
same equipartition-based definition.

We begin with liquid water. Figure 1 shows the time-
resolved VDOS for excited and non-excited molecules.

Immediately after excitation, a pronounced enhancement
of spectral intensity appears in the O–H stretching re-
gion, confirming the effective population of the targeted
vibrational states. Notably, the initial peak is centered
at a slightly lower frequency than the maximum of the
equilibrium stretching band, reflecting the fundamen-
tal frequency of the isolated Lippincott–Schroeder po-
tential used in the Wigner initialization. As the sys-
tem evolves, the stretching feature progressively shifts
toward higher frequencies, approaching the equilibrium
band position. This shift indicates the gradual adapta-
tion of the initially prepared molecular-like excitation to
the condensed-phase environment.

IV. CONCLUSIONS

[1] M. Matsumoto, T. Yagasaki, and H. Tanaka, Journal of Computational Chemistry **39**, 61 (2017).

[2] Z. Chen, M. L. Berrens, K.-T. Chan, Z. Fan, and D. Donadio, Journal of Chemical & Engineering Data **69**, 128 (2023).

[3] K. Ando, The Journal of chemical physics **125** (2006).